Carbon derived from silicon carbide fibers, a comparative study

*Stéphane Mazerat, Joséphine Lacroix, Benoît Rufino, René Pailler**

University of Bordeaux, Laboratoire des Composites ThermoStructuraux, UMR 5801 (CNRS - UB - Groupe SAFRAN - CEA), 3 allée de la Boetie, 33600 Pessac, France

Dr. Stéphane Mazerat
Laboratoire des Composites Thermostructuraux (LCTS), UMR 5801, CNRS-SAFRAN-CEA-UB, 3 allée de la Boétie, 33600 Pessac, France[1]

Dr. Joséphine Lacroix
Laboratoire des Composites Thermostructuraux (LCTS), UMR 5801, CNRS-SAFRAN-CEA-UB, 3 allée de la Boétie, 33600 Pessac, France

Dr. Benoît Rufino
Laboratoire des Composites Thermostructuraux (LCTS), UMR 5801, CNRS-SAFRAN-CEA-UB, 3 allée de la Boétie, 33600 Pessac, France

Dr. René Pailler
Laboratoire des Composites Thermostructuraux (LCTS), UMR 5801, CNRS-SAFRAN-CEA-UB, 3 allée de la Boétie, 33600 Pessac, France
** Corresponding author: Phone: +33 556 844 733; Fax: +33 556 841 225; E-mail address: pailler@lcts.u-bordeaux.fr*

Introduction sentence

The paper reports a comparative study between various SiC-based fibers (11 in total) and their corresponding derived carbon, obtained by chlorination treatment at intermediate temperatures. The so obtained carbide derived carbons (CDC) are mainly microporous, but some substrates, such as high oxygen containing or third-generation SiC fibers, also show some mesoporosity. The CDC pore size distribution is found to be related to fibers chemical composition. Moreover, because the carbon free of fibers is not affected by the treatment in the selected etching condition, the percolation and amount of this former network remain intact and are correlated with CDC mechanical properties, respectively the tensile strength and the Young modulus. Hence, an analogy between SiC-based fibers derived carbon and a composite material can be proposed.

Introduction 30 words

Carbon derived from silicon carbide-based fibers is micro-mesoporous with size distribution related to the substrate chemical composition and composite-like mechanical properties: amorphous SiC/SiCO-derived carbon reinforced with sp2 carbon-free network.

Graphical abstract

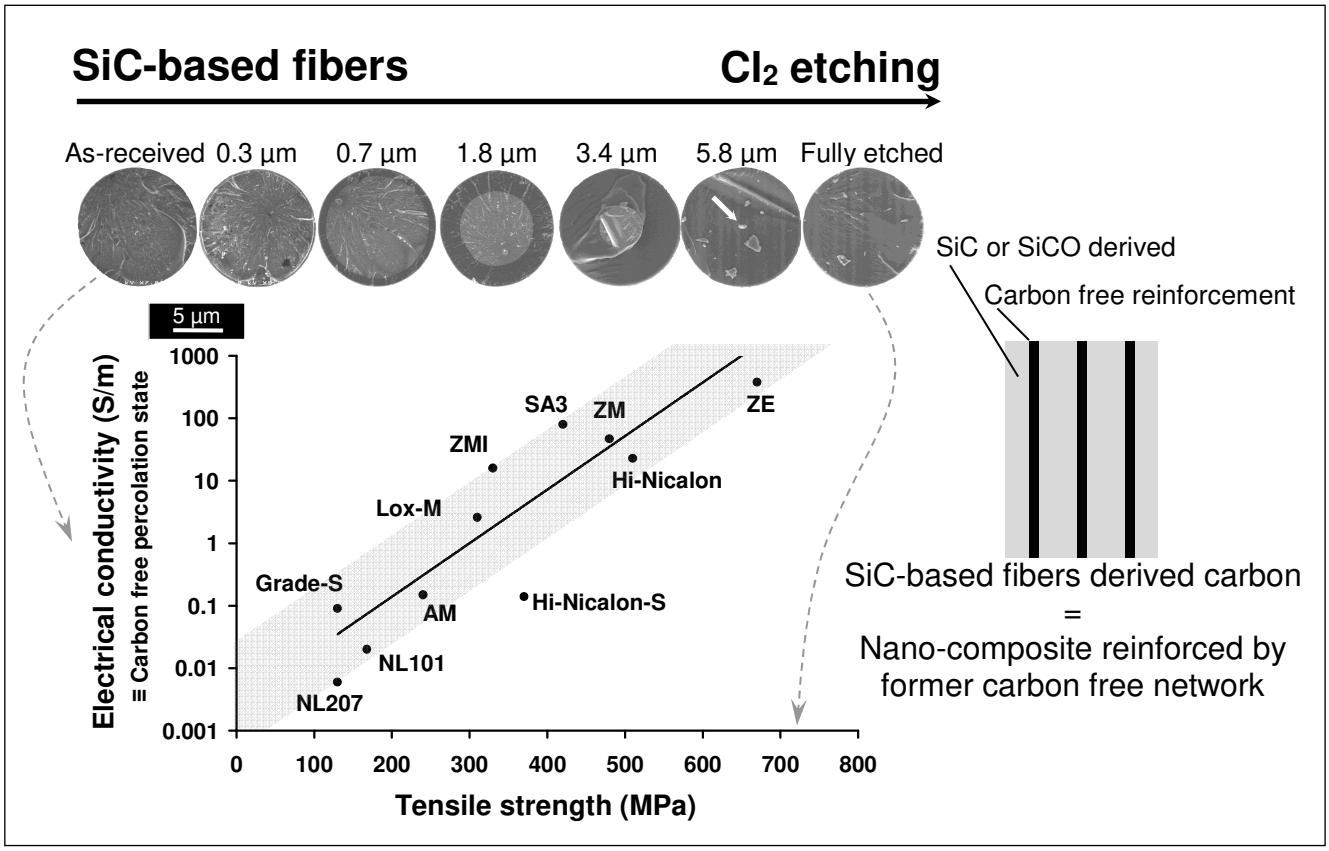

Authors

Dr. Stéphane Mazerat
Laboratoire des Composites Thermostructuraux (LCTS), UMR 5801, CNRS-SAFRAN-CEA-UB
3 allée de la Boétie, 33600 Pessac, France[1]

[1] Present adress: 41 rue du Quesnoy 59570 Bavay, France

Dr. Joséphine Lacroix
Laboratoire des Composites Thermostructuraux (LCTS), UMR 5801, CNRS-SAFRAN-CEA-UB
3 allée de la Boétie, 33600 Pessac, France

Dr. Benoît Rufino
Laboratoire des Composites Thermostructuraux (LCTS), UMR 5801, CNRS-SAFRAN-CEA-UB
3 allée de la Boétie, 33600 Pessac, France

Dr. René Pailler
Laboratoire des Composites Thermostructuraux (LCTS), UMR 5801, CNRS-SAFRAN-CEA-UB
3 allée de la Boétie, 33600 Pessac, France

E-Mail: pailler@lcts.u-bordeaux.fr
Tel: +33 5 56 84 47 33
Fax: +33 5 56 84 12 25

Dr. René Pailler
University of Bordeaux
LCTS - Lab for Thermostructural Composites

To Dr De Geuser
Editor
Materials Today Communications

Dear Dr De Geuser

Please find hereby attached a manuscript entitled: “Carbon derived from silicon carbide fibers, a comparative study”, by S. Mazerat, J. Lacroix, B. Rufino and myself, initially submitted to Carbon with a transfer offer to your journal. You will find at the end of this cover letter the reviewers comments, taken into account in the submitted manuscript.

Main points

Carbide-derived carbon (CDC) materials are in view for a variety of applications such as gas storage, supercapacitor or catalysis. They have been produced by different etching treatments, the main reported being the halogenation (chlorination for instance), of different carbides with a simple concept: selectively etch metallic atoms leaving an amorphous carbon skeleton. Some authors report partial surface transformation of SiC-based fibers into CDC coating for direct or indirect interphase coating synthesis in ceramic matrix composite (CMC). Nevertheless, no studies treated the characterization of fully transformed fibers. The present study compares the as-received fibers chemical composition, microstructure and electrical conductivity respectively with the resulting CDC porosity, chemical stability toward oxidation and mechanical properties.

A total of eleven different SiC-based fibers were selected for this study. They belong to the first (oxygen cured), second (electron beam cured) or third (pyrolyzed at high temperature) generations, with various microstructures and chemical compositions. The treatment took place at atmospheric pressure and intermediate temperatures (550 °-850 °C range) under pure chlorine flow. Overall, the results showed a significant relationship between the oxygen content of the former fiber and their derived carbon pore size distribution. Moreover, CDC tensile properties were found to be related to the former carbon free network, hence revealing a composite-like behavior.

This study is the first, for our knowledge, to investigate the tensile mechanical properties of these carbon materials, revealing the benefit of a non-etched network, reinforcing the CDC. Together with pore-size distribution tuning, selecting the proper etching condition or substrate composition, this work is of high interest for application targeting high specific surface areas (> 1000 $m^2\ g^{-1}$) carbons with specific mechanical behavior.

We confirm that this manuscript has not been published elsewhere and is not under consideration by another journal. All authors have approved the manuscript and agree with its submission to Carbon. This study was funded by Safran Ceramics. The authors have no conflicts of interest to declare.

For a peer review process, we would like to recommend some of the following possible referees who are well known in the background research field of this article.

Dr. Q. Ma
Science and Technology on Advanced Ceramic Fibers & Composites Laboratory
National University of Defense Technology
Changsha 410073 China
Phone: +86 731 84573162
E-Mail: nudtmqs1975@163.com

Prof. K. Guerin
Laboratoire des Matériaux Inorganiques
UMR CNRS 6002-Université Blaise Pascal
24 av. des Landais, 63177 Aubière Cedex France
Phone: +33 (0)4 73 40 75 67
E-Mail: katia.araujo_da_silva@uca.fr

Prof. N. Popovska-Leipertz
Department of Chemical and Biological Engineering
University Erlangen-Nuremberg
Egerlandstraße 3, 91058 Erlangen Germany
Phone: +49 9131 85 27420
E-Mail: nadejda.leipertz.popovska@fau.de

Prof. F. Rodriguez Reinoso
Laboratorio de Materiales Avanzados, Departamento de Quimica Inorgánica
Universidad de Alicante Apartado 99, E-03080 Alicante Spain
Phone: +34 965 903 544
E-mail: reinoso@ua.es

Prof. Y. Gogotsi
Trustee Chair Professor of Materials Science and Engineering
Director, A.J. Drexel Nanotechnology Institute, Drexel University
3141 Chestnut St Philadelphia, PA 19104 USA
Phone: 215 895 6446
Fax: 215 895 1934
E-mail: gogotsi@drexel.edu

Reviewers comments from Carbon:

Reviewer #1: This manuscript describes a comparative study of carbon derived from silicon carbide fibers. The authors carefully performed experiments, and the results obtained were analyzed and discussed systematically and rationally. A weak point of this manuscript is the appeal of the significance of the conclusions induced from the experiments. All the results are reasonable, but in turn they look commonplaces. I would suggest the authors to describe how the findings are valuable and can contribute to the advances of the relevant field at the introduction.
Other specific comment is shown below:

1. Table 1: Please insert a footnote as for the method used for the determination of Si/C/O/X compositions as well as the ratio of SiC and SiCO.
2. In equation (4), the authors calculate the free carbon atomic content (%Cfree) by subtracting the amount of carbon in SiC (%Si) and SiO2 (%O/2) from the total carbon amount (%C). However in Table 1, the amount of SiCO is shown instead of SiO2. Is it possible to obtain the amount of SiO2 from SiCO? If so, please describe the method.
3. Please clearly define the parameter Ø<beta>-SiC, in Table 1. Additionally, please describe how the authors determined it.
4. "Subsequently to chlorination treatment, the cross section of some fibers was observed by scanning electron microscopy (SEM Hitachi S4500) to confirm their complete transformation (no chemical contrast by SEM) (Fig. 1)." The contrast observed by SEM would be due to the difference in conductivities in C and SiC matrices, rather than chemical contrast. Charge build up is more significant on the insulative SiC surface.
5. As shown in Table 2, different chlorination temperatures are used for different samples. Please describe the reason for selecting these temperatures for each.
6. "Brunauer-Emmet-Teller" should be "Brunauer-Emmett-Teller".
7. P6: "pores sizes" should be "pore sizes".
8. As the authors are aware of the fact, use of SiC isotherm for alfa-s analysis of porous carbon is not appropriate. Instead, non-porous carbon like carbon black should be used as a standard.

Reviewer #2: The manuscript studies the preparation of porous carbons from silicon carbide fibers by the well-known method of heat treatment with chlorine. The authors prepared a variety of porous carbon fibers and have made a detailed characterization of porosity and mechanical properties, among others. The authors have demonstrated that this methodology can be successfully applied to obtain CDC fibers with different properties. Considering that the preparation method is not novel and that the main outcome is a series of porous carbon fibers derived from SiC fibers which properties are not very different to those of conventional activated carbon fibers, I cannot recommend this manuscript for publication in Carbon.

Carbon derived from silicon carbide fibers, a comparative study

*Stéphane Mazerat, Joséphine Lacroix, Benoît Rufino, René Pailler**

University of Bordeaux, Laboratoire des Composites ThermoStructuraux, UMR 5801 (CNRS - UB - Groupe SAFRAN - CEA), 3 allée de la Boetie, 33600 Pessac, France

** Corresponding author: Phone: +33 556 844 733; Fax: +33 556 841 225; E-mail address: pailler@lcts.u-bordeaux.fr*

Abstract

SiC-based fibers, eleven in total, derived from polycarbosilane pyrolysis and belonging to the three different generations, were fully converted into microporous carbon after selective etching of silicon atoms under pure chlorine flow at intermediate temperatures (550 °-850 °C). In this work, relationship between as-received fibers and their subsequent carbide-derived carbon (CDC) properties, pore structure oxidation resistance and mechanical properties, was investigated. The resulting carbon is microporous or micro-mesoporous with equivalent specific surface area exceeding 1000 m^2 g^{-1} and pore size distribution (PSD) related to the substrate chemical composition and microstructure of former fibers. Oxidation kinetics were found to depend on this PSD. The former sp2 carbon free network of fibers remained unaffected by the chlorination. Its amount and percolation were respectively correlated to Young modulus and tensile strength of CDC. This carbon thus displays a nano-composite-like behavior with a former etched carbide matrix (transformed SiC and SiCO) and carbon free reinforcement. The results demonstrate CDC allows the control over pore size and mechanical properties by selecting an appropriate multiphasic substrate, combining etched and non-etched compounds.

1. Introduction

In the last two decades, carbide-derived carbon (CDC) has gained much attention for many applications like gas storage, adsorbent, catalyst support, electrode or supercapacitor. They are produced by extraction, layer by layer, of metallic atoms from carbide leaving a carbon skeleton. This is processed by halogenation at intermediate or high temperature, resulting in the formation of volatile halides [1–2]. CDC has been obtained from different carbides: SiC [3], TiC, ZrC, B_4C, Al_4C_3 [4–6], Fe_3C [7] and many others [8], silicon carbide being the most reported. CDC are porous materials with tunable pore size distribution (PSD), from micro to mesoporosity with a sub−Ångstrom accuracy, depending on the treatment temperature, the carbide precursor or its microstructure [6, 8–15]. Pure chlorine [16−19], diluted in Ar or H_2 [3, 12] or HCl [20], is the most reported halogen element to produce this material, even if fluorine [21], bromide or iodine can be used as well. In the case of silicon carbide chlorination at intermediate temperatures and ambient pressure, carbon does not react with chlorine to form $CCl_{4(l\ or\ g)}$ [1]. Process is associated with the following equation:

$$SiC_{(s)} + 2Cl_{2(g)} \rightarrow SiCl_{4(g)} + C_{(s)} \quad (1)$$

C. Vakifahmetoglu et al. used silicon oxycarbide (SiCO) materials to produce CDC [22]. The reaction involved can be written as follows:

$$SiC_xO_y + 2Cl_2 \rightarrow SiCl_4 + (x\text{-}y/2)C + y/2CO_2 \quad (2)$$

$$SiC_xO_y + 2Cl_2 \rightarrow SiCl_4 + (x\text{-}y)C + yCO \quad (3)$$

The oxygen content of these materials presents a particular interest: it increases the pore size and acts as a well-controlled *in-situ* activation agent, which contrast with CO_2 [23–25] or KOH [26] post treatment agents. Firstly, CDC is prone to oxidation at low temperature range, down to 225 °C [17], because of its disordered microstructure [5, 12, 27]. Secondly, the mixed silicon atoms environment (SiC_3O, SiC_2O_2 or $SiCO_3$) destabilizes the structure and enhance its sensitivity to Cl_2 [18, 22]. This later result is consistent with chlorination kinetics of first-generation SiC-based fibers. Nevertheless, only few authors studied this kind of material [16–18, 28–31]. They are commercially available and display various and well documented chemical or microstructural properties, useful for fundamental research, with a flexible filament shape prone to tensile testing. The mechanical properties of CDC coatings are usually assessed, for tribological purpose [32–35], by nanoindentation showing a Young modulus about 5 GPa [36]. To our knowledge, no studies deal with totally transformed SiC-based fibers characterization. The aim of this work is to produce CDC from eleven different

SiC-based fibers and compare some physicochemical and mechanical properties of the derived carbon (DC) with the precursor ones.

2. Materials and method

2.1 Materials

Silicon carbide fibers are synthesized by the conversion of polycarbosilane (PCS, commercialized by Nippon carbon Co. Ltd. under the trade name Nicalon®), or derivate containing small amount of organometallic (polytitanocarbosilane PTCS, polyzirconocarbosilane PZCS or polyaluminocarbosilane PACS commercialized by UBE Industries Ltd. under the trade name Tyranno®). The first-generation fibers are oxygen cured and thus composed of a silicon oxycarbide phase (SiCO) embedding SiC grains in nanometer range and free aromatic carbon as basic structural units (BSU) [37]. This free carbon atomic content is approximated (considering only SiC and SiO_2 phases) from:

$$\%C_{free} = \%C - \%Si + \frac{\%O}{2} \quad (4)$$

Seven studied fibers belong to this first-generation: two without metallic element (NL101 and NL207), two doped with titanium (Grade-S and Lox-M), two other containing zirconium (ZMI and ZM) and the last one with aluminum (AM). Hi-Nicalon (referred as Hi-Ni) and ZE (containing Zr) belong to the second, whereas Hi-Nicalon type S (referred as Hi-Ni-S) and SA3 (aluminum doped) belong to the third-generation SiC-based fibers. Second-generation fibers are electron beam cured and thus show lower oxygen content, whereas the third-generation underwent a high temperature treatment (CO degassing of AM or decarbonating under H_2 of Hi-Ni precursors) followed by sintering about 1800 °C [38]. The fibers from this latter generation are nearly stoichiometric with larger SiC grain sizes. A total of eleven different fibers were so investigated (Table 1).

	Fiber	Diameter (µm)	Si	C	O	X	C_{free}	SiC	SiCO	C_{free}	Ø β-SiC (nm)
			(at.%)					(vol.%)			
1st Generation	NL101	15	36.4	46.8	16.7	-	18.8	26	30	44	1.2
	NL207	14	38.6	48.6	12.8	-	16.4	36	25	39	1.9
	Grade-S	8.5	31.8	48.1	19.4	Ti: 0.7	26.0	19	27	54	1.2
	Lox-M	11	35.4	53.3	10.4	Ti: 0.9	23.1	41	8	51	1.9
	ZMI	11	35.5	54.3	10.0	Zr: 0.2	23.9	43	6	52	2.2
	ZM	11	34.7	56.5	8.6	Zr: 0.2	26.0	42	3	55	2.5
	AM	11	32.9	52.5	14.2	Al: 0.4	26.7	28	17	55	2.2
2nd	Hi-Ni	14	41.9	57.2	0.9	-	15.8	61	0	39	5.0
	ZE	11	36.3	61.9	1.7	Zr: 0.1	26.4	45	0	55	3.5
3rd	Hi-Ni-S	12	48.7	51.0	0.3	-	2.6	85	0	15	50
	SA3	10	47.8	52.4	0.3	Al: 0.5	4.7	85	0	15	300

Table 1: Chemical composition, phase volume proportion and microstructure of the selected silicon carbide fibers [30-31,39]. Chemical composition was measured at CNRS facility in Solaize by ICP-AES and oxidation [39]. The amount of crystallized β-SiC was determined by X-Ray diffraction (XRD) and the mean size (Ø β-SiC) assessed by the Scherrer formulae. The amount of SiCO infers from difference between chemical composition and quantity of β-SiC and C_{free}.

2.2 Chlorination treatment

Prior to any treatment, SiC-based fibers were desized at 650 °C for 10 min in air, followed by thin silica film removal in 10 vol.% hydrofluoric acid bath for 4 minutes. The chlorination was performed in a horizontal silica tube (Ø = 70 mm) heated by a 3-zones resistive furnace (Carbolite Ltd.) described elsewhere [17–19, 30–31]. Specimens were placed in the 250 mm hot isothermal zone. The tube tightness was checked under static vacuum, set by fore line pump, over a night. The reactor was then filled with pure chlorine and heated up with a linear ramp of 20 °C min^{-1}. Once atmospheric pressure reached, Cl_2 flow rate was set to 0.6 NL min^{-1} and outlet opened. Excess of chlorine and products of the reaction were trapped in 2 successive 1 L washing bottles of NaOH (2 mol L^{-1}). The trapping system could be interchanged to a second parallel outlet. This manipulation was necessary for cleaning purpose, when the NaOH solution was saturated (Equation 5) or the output obstructed by silica gel (hydrolysis of $SiCl_4$), without disturbing the gas flow or pressure during the treatment.

$$Cl_2 + 4NaOH \rightarrow 2NaCl + 2NaClO + 2H_2O \quad (5)$$

Two distinct treatment protocols were used to produce CDC. The first one aimed to transform 60 mm long multifilament tows, for tensile tests purpose. A two hours annealing at 850 °C

was selected to suit the reactivity of all fiber types. The second protocol aimed to transform larger samples to obtain 200-300 mg of CDC for further characterization. It was therefore performed on 2D woven (150 x 30 mm) or tows with adequate length. The treatment settings were selected to limit the kinetic and silica gel formation rate at the outlet, for obvious safety reasons. The treatment was hence divided in two steps: (i) etching of the firsts 3 µm in 1 hour selecting properly the temperature (T1) according to chlorination kinetics [18, 30–31], (ii) followed by another hour at T2 = T1 + 25 °C (about twice the transformation kinetic observed at T1) to complete the core transformation (Table 2). This protocol assumes the etching depth is proportional to the annealing duration, confirmed elsewhere for fiber sample size [2, 16–17, 30, 40]. Subsequently to chlorination treatment, the cross section of some fibers was observed by scanning electron microscopy (SEM Hitachi S4500) to confirm their complete transformation (no difference in charge build up by SEM) (Fig. 1). The hypothesis is made that CDC remains amorphous in this temperature range (T < 900 °C) [4–5, 12, 27].

Sample	Chlorination temperature (°C)	
	T1	T2
NL101-DC	650	675
NL207-DC	650	675
Grade-S-DC	550	575
Lox-M-DC	625	650
ZMI-DC	675	700
ZM-DC	700	725
AM-DC	700	725
Hi-Ni-DC	825	850
ZE-DC	775	800
Hi-Ni-S-DC	825	850
SA3-DC	825	850

Table 2: Chlorination treatment temperatures (first hour at T1, 3µm etching, and second hour at T2=T1+25 °C) used to fully transform tow/woven of SiC fibers for subsequent physisorption and oxidation analysis.

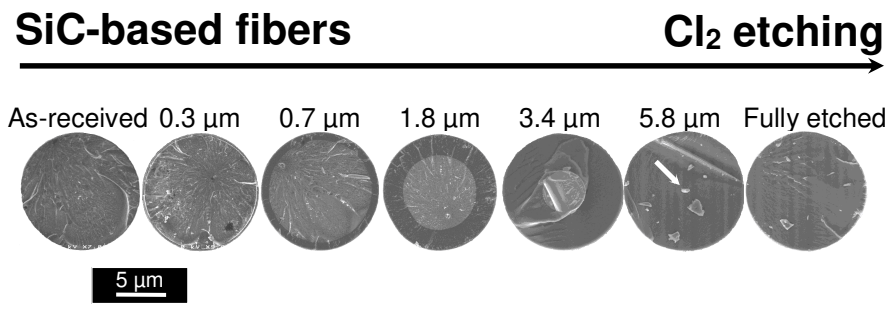

Fig. 1: SEM observation of fiber section after chlorination treatment showing its progressive transformation into CDC as the treatment duration increases. Fully transformed fibers were considered for this work (arrow show the untransformed fiber core).

At the end of annealing time, furnace was turned-off and a nitrogen purge (1.2 NL min^{-1}) initiated. Previous works performed on SiC or SiCO samples revealed that under atmospheric pressure, chlorine extraction from porosity begins at 600 °C [9–10, 12–13, 17, 19, 30]. This was found to result in effective micropore volume and equivalent specific surface area enhancement to respectively 33% and 25% [29]. Hence, depending on chlorination temperature, a bias in CDC porosity can be anticipated. Therefore, to reliably compare the different carbons, a second annealing treatment was initiated, once the system purged, for 1 hour at 700 °C under dynamic primary vacuum.

2.3 Physico-chemical characterization

The electrical conductivity (σ, S m^{-1}) of as-received fibers was measured on desized bundles comprising four or five tows (corresponding to several thousands of fibers) with a four-points testing device described elsewhere [41]. Copper wires were connected to bundle using silver painting. The sample section (S_0) was calculated according to the following equation:

$$S_0 = \frac{m_0}{L_0 \rho} \quad (6)$$

Where ρ is the fiber density (Helium pycnometer, Micromeritics Co., AccuPyc II 1300), m_0 and L_0 are the bundle mass and length respectively.

Nitrogen adsorption analysis was carried out on fully transformed fibers, using a commercial Micromeretics ASAP 2010 at 77 K with equilibration intervals of 10 s. Because of the hygroscopic nature of CDC, air contaminants, like moisture, are rapidly adsorbed in porosity and could disturb gas physisorption measurements. Hence transformed woven were directly outgassed at 300 °C under secondary vacuum for twelve hours, just after chlorination oven opening. The equivalent specific surface area (SSA in m^2 g^{-1}) and the C parameter inferred from Brunauer-Emmett-Teller (BET) equation [42] for $P/P_0 < 0.3$, with an upper partial pressure range adjusted to ensure $R^2 > 0.999$. Effective micropore volume and size distribution were calculated using the semi-empirical Horvath-Kawazoe (H-K) approach [43] with slit pore geometry. Micropores could further be subdivided into ultramicropores (pore width < 0.7 nm) and supermicropores (0.7 nm < pore width < 2 nm) [44]. These latter pore

sizes were characterized with alpha-s method, developed by K.S.W. Sing et al. [45–49]. For that purpose, isotherm of non-porous carbon [50] (SSA = 8.70 $m^2\ g^{-1}$) was taken as reference and normalized by its adsorption at $P/P_0 = 0.4$. The mesopore size distribution (meso-PSD) was calculated by Barret-Joyner-Halenda (BJH) method [51] based on a modified Kelvin equation. This method account for partial pressures above 0.45 and pores larger than 40 Å. Single point total pore volume ($V_{p,0.99}$) was assessed using the Gurvich rule, determined from the specific amount of gas adsorbed at a relative pressure close to the saturation vapor pressure ($0.90 < P/P_0 < 0.99$), with a density conversion factor of 1.5468×10^{-3} $cm^3\ cm^{-3}$ (STP) [45, 52].

Thermogravimetric analysis (TAG 24, Setaram Inc.) was used to study the fiber derived carbon (fiber-DC) oxidation kinetics under pure dry oxygen flow (60 NmL min^{-1}) with a linear ramp of 5 °C min^{-1} until 650 °C. Sample of approximately 50 mg were placed in alumina crucible and outgassed under primary vacuum at room temperature for several minutes prior to oxidation. TGA experiments were performed just after nitrogen adsorption analysis for the same contamination reasons whereas mechanical testing did not require such precautions.

2.4 Mechanical characterization

Room temperature mechanical properties were measured by tensile tests of either sized as-received (40-50 tests) or fully transformed (20 tests) monofilaments, with a dedicated machine [53]. Samples were individually pulled out from tows and glued on a paper holder with a 25 mm window [54]. Special care needed to be taken for manipulation of CDC specimen, because of their low density and stiffness. CDC sample kept, after treatment, the woven geometry and therefore undulated. Therefore, a slight force was applied to sample to force it to be straight and ensure axial gluing to paper holder. Fibers diameter was measured, prior to testing, using their laser diffraction pattern [55]. Once gripped in the device, the paper holder was cut on both sides. Tensile tests were carried out at a constant elongation rate (0.5 % min^{-1}). The applied load and displacement were respectively measured using load cell (0–2 N) and LVDT extensometer, mounted on the grips. The measured elongation was corrected accounting for the system compliance, ascertained with 10 extra tests at 10 and 40 mm gauge lengths.

3. Results and discussion

3.1 SiC-based fibers properties

Some properties of as-received fibers, such as their chemical composition, phase volume proportion, β-SiC grain size, density (ρ), mechanical properties, and electrical conductivity (σ) are reported in Tables 1 and 3 [30–31, 39]. These fibers display a wide range of composition, from first-generation with high oxygen content (NL101 or Grade-S with respectively 16.7 and 19.4 at.% O) to the near stoichiometric third-generation (Hi-Ni-S and SA3), through intermediate fibers with oxygen content around 10 at.% (Lox-M and ZMI) or lower like ZM (8.6 at.% O) and ZE (1.7 at.% O). The β-SiC mean grain size is otherwise correlated to the oxygen content: higher the oxygen content is, lower SiC crystallite sizes are [38, 56]. This latter comment need to account for manufacturing pyrolysis temperature, excess of carbon and heteroelement nature. For example, titanium is used to inhibit SiC grains growth.

Fiber	Mechanical properties ± std. dev.				Physical properties	
	Tensile strength (GPa)	Elongation (%)	Young modulus (GPa)	$E_{(mixture\ rule)}$ (GPa)	σ ($S\ m^{-1}$)	ρ ($g\ cm^{-3}$)
NL101	2.2 ± 0.6	1.2 ± 0.3	180 ± 13	190	0.02	2.57
NL207	2.8 ± 0.7	1.3 ± 0.3	210 ± 20	220	0.006	2.58
Grade-S	2.8 ± 0.6	1.5 ± 0.3	180 ± 10	150	0.09	2.35
Lox-M	3.0 ± 0.7	1.5 ± 0.3	200 ± 10	220	2.6	2.37
ZMI	3.1 ± 0.7	1.5 ± 0.3	210 ± 20	220	16	2.48
ZM	3.4 ± 0.7	1.6 ± 0.3	220 ± 10	220	47	2.48
AM	3.0 ± 0.5	1.6 ± 0.2	180 ± 12	180	0.15	2.42
Hi-Ni	3.0 ±0.4	1.0 ± 0.1	300 ± 20	300	32	2.74
ZE	3.3 ± 0.7	1.5 ± 0.3	230 ± 18	230	380	2.55
Hi-Ni-S	2.9 ± 0.4	0.6 ± 0.1	470 ± 45	400	0.14	3.05
SA3	2.8 ± 0.5	0.7 ± 0.3	420 ± 20	400	80	3.00

Table 3: Details of mechanical and physical properties of the as-received SiC-based fibers.

The electrical conductivity of a SiC-based fiber is ascribed to the percolation state of its free carbon network. Indeed, BSU is a conductive phase embedded in a relatively insulating continuum (SiC and SiCO) [57, 41]. The family of electrically conductive fibers gathers ZMI, ZM, ZE, Hi-Ni and SA3. However, NL101, NL207, Grade-S, AM, Hi-Ni-S are electrically insulative. The Lox-M fiber is intermediate between these two families (Table 3). Except for third-generation, all fibers contain a large amount of carbon-free, exceeding 15 atomic percents. Tyranno® fibers are C_{free} rich in comparison to Nicalon® ones (Table 1), but this amount does not account for its continuity. The discrepancy existing between Hi-Ni-S (insulative) and SA3 (conductive) fibers can be ascribed to the radial gradient of carbon

content in the latter one [58]. As mentioned before, free carbon excess on fiber is not likely to be transformed by chlorine in the selected temperature range.

SiC-based fibers display a brittle mechanical behavior with a Young modulus dictated by the rule of mixture, knowing volume proportion (V_x Table 1) of each phase:

$$E_{fiber} = E_{SiC}.V_{SiC} + E_C.V_C + E_{SiCO}.V_{SiCO} \quad (7)$$

As an assumption, the SiC Young modulus (E_{SiC}) is set to the Hi-Ni-S fiber one (470 GPa). Best fitting is found considering elastic moduli of 28 GPa and 175 GPa for carbon free and SiCO phases respectively, with a scattering below 17% (Table 3). The impact of manufacturing route, curing and annealing temperatures on C_{free} and SiCO Young moduli and intrinsic β-SiC grain size partly explain this scattering. This method is naturally an approximation of the inner phase properties. It is worth to note the estimated SiCO modulus is close to oxygen rich fibers.

3.2 SiC-based fiber-DC elaboration

As mentioned in method section, CDC thickness is proportional to the etching duration (Equation 8) [16–18, 29, 31, 40, 59] in this range of sample size [2], revealing the etching reaction is not piloted by reactant or product transportation to or from the reaction interface. Kinetics evolution with temperature obeys the Arrhenius law (Equation 9).

$$e = kt \quad (8)$$

$$k = k_0 e^{-Ea/RT} \quad (9)$$

where e is the CDC thickness (nm), k the reaction rate (nm s^{-1}), t the treatment duration (s), k_0 the pre-exponential factor (nm s^{-1}), E_a the activation energy (J mol^{-1}) (Table 4), R the universal gas constant (8.314 mol J^{-1} K^{-1}) and T the temperature (K). It is worthwhile noting transformation kinetics of SA3 fibers is not reported because of etching depth inconsistency, presumed to occur preferentially at grain boundaries [30–31, 53].

	Fiber	Ea ± std. dev. (kJ mol^{-1})	k_0 (nm s^{-1})
Nicalon®	NL101	128 ± 8	1.3 x 10^7
	NL207	132 ± 4	9.0 x 10^6
	Hi-Ni	280 ± 10	8.8 x 10^{12}
	Hi-Ni-S	322 ± 50	3.1 x 10^{14}
Tyra	Grade-S	106 ± 7	2.2 x 10^6
	Lox-M	152 ± 10	2.8 x 10^8

ZMI	211 ± 10	2.5 x 10^{11}
ZM	237 ± 8	3.2 x 10^{12}
ZE	340 ± 10	7.1 x 10^{16}
AM	163 ± 5	2.8 x 10^{8}

Table 4: Arrhenius parameters describing the kinetics of SiC-based fibers etching by pure chlorine at intermediate temperatures (550 °-850 °C).

As mentioned before, two experimental procedures were used. Samples for mechanical testing were treated in the same conditions whereas large samples were transformed at two successive temperatures depending on their reactivity against chlorine. The treatment temperature strongly depends on fiber type (Table 2), based on their transformation kinetics (Table 4). For instance, Grade-S was fully converted in CDC at 575 °C while Hi-Ni had to be handled at 850 °C for the same result. The oxygen amount and the nature of metallic heteroelement, when present, are found to play a critical role on the fiber reactivity (Table 4), and more likely on the SiCO phase [18, 30–31]: titanium (Grade-S and Lox-M) enhanced it (lower Ea) whereas zirconium (ZMI, ZM, ZE) or aluminum (AM) reduced it (higher Ea).
The SiC-fiber-derived carbon was found to have a shape memory of the geometry during the treatment. Indeed, fibers-DC, when extracted from a treated woven, keep the geometry it had during Si atoms extraction and undulate whereas as-received fibers are straight.

3.3 Physisorption experiments

SiC-fibers-DC display significant adsorbed volume at low relative pressure (Fig. 2) typical for type-I isotherm according to the IUPAC classification and characteristic of microporous samples (pore width < 2 nm) [52]. Despite the same classification for all samples, adsorption isotherms can be separated into four (4) shapes:

- Shape A, nitrogen is adsorbed on a wide range of partial pressure until the mesopororosity limit ($P/P_0 = 0.4$) [60]. This indicates a broad micropore size distribution (Figs. 2.a and 3.a). This shape gathers carbons derived from all first-generation fibers (oxygen cured) excepting NL101-DC.
- Shape A*, nitrogen adsorption isotherm curve is shape A-like below 0.4 P/P_0 but displays an H2a-like [52] single steeped hysteresis loop ($0.4 < P/P_0 < 0.55$). This behavior is typical for mesoporous materials (type IV isotherm according to IUPAC classification) exhibiting pore sizes between 2 and 50 nm (Fig. 3.b). The partial pressure for which loop is closed (0.45 P/P_0) indicates a cavitation controlled evaporation of the capillary condensate from mesopores, that

is obstructed by the pore constriction (ink bottle-like with neck size < 4 nm) [44–45, 52]. This phenomenon can be related to the adsorbate nature (carbon wall), temperature and cavities linked to micropores. The first generation NL101-DC displays this isotherm shape (Fig. 2.a).

- Shape B, nitrogen is adsorbed on a sharp partial pressure domain, showing narrow micropore size distribution (Figs. 2.b and 3.a). Isotherms of the second-generation fibers-DC belong to this shape (Hi-Ni-DC, ZE-DC).

- Shape B*, nitrogen adsorption isotherm curve is shape B-like below 0.4 partial pressure. It is characterized by a single steeped hysteresis loop between adsorption and desorption branches, H2a-like ($0.4 < P/P_0 < 0.9$) closing at 0.4-0.5 P/P_0 (Fig. 2.b), typical for mesoporous material (Fig. 3.c). Consequent pore structure is similar to shape A* mentioned before. The CDC derived from third-generation fibers (Hi-Ni-S-DC and SA3-DC) exhibits this isotherm shape.

ZM-DC and ZE-DC are respectively classified as shape A and B but seem more likely intermediate: nitrogen is adsorbed up to 0.2-0.3 partial pressure. This could be linked to their oxygen level, also intermediate between first-generation and Hi-Ni-DC, as will be discussed later.

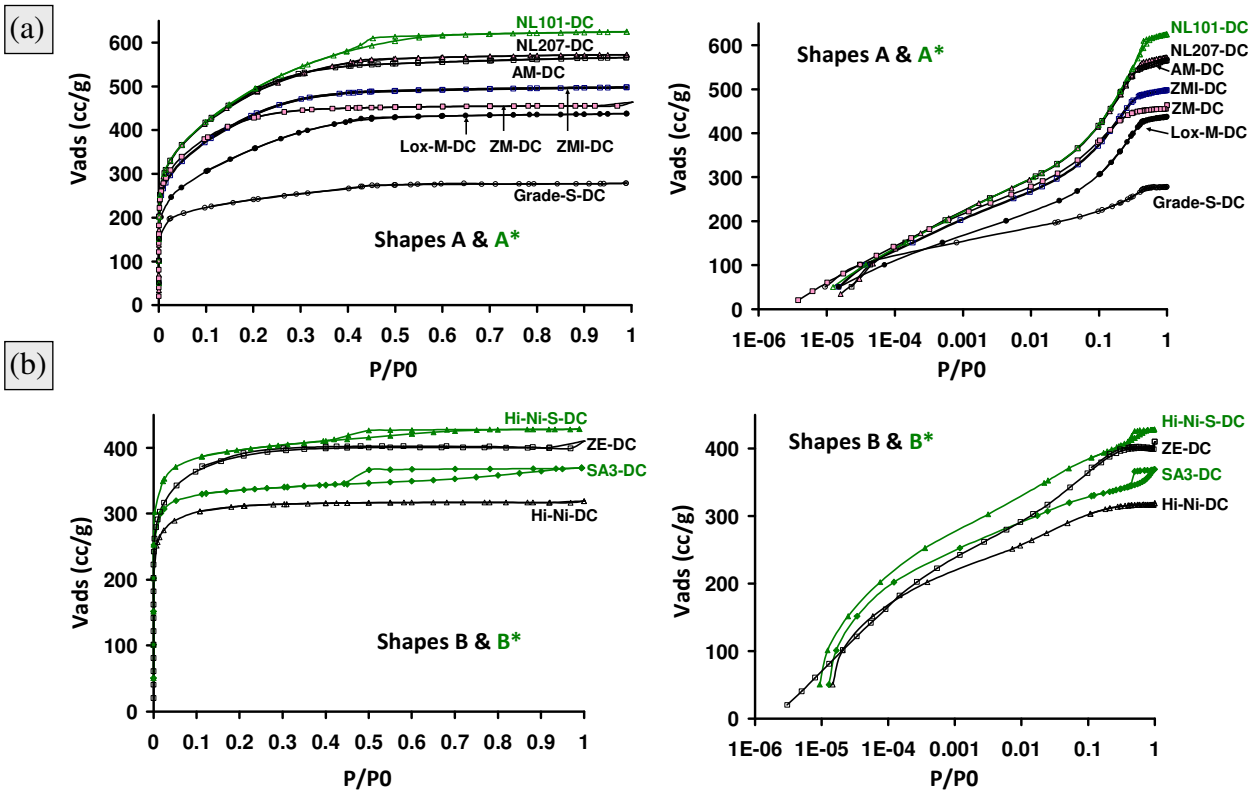

Fig. 2: Nitrogen physisorption isotherms for SiC-based fibers fully transformed in CDC after chlorine etching treatment displaying (a), broad micropore size without (shape A) or with

(shape A*) mesopores, (b), narrow micropore size (shape B) or micro-mesoporosity (shape B*).

Table 5 summarizes pore structure properties for all here studied CDC. Excepting for Grade-S-DC, equivalent specific surface area (SSA) ranges from 1100 to 1800 $m^2\ g^{-1}$, associated with effective micropore volume (H-K method) from 0.5 to 0.8 $cm^3\ g^{-1}$. Some mesopority is also identified with limited volume according to BJH method (taking account for pore larger than 40 Å from adsorption branch). CDC can thus be considered as mostly microporous. These properties agree with previous works performed on SiC-based fibers chlorination etching [17, 29] but do not reach values calculated on SiCO-DC (> 2000 $m^2\ g^{-1}$) [22]. A higher temperature for carbide halogenation has often been reported to increase the SSA, the effective micropore volume and PSD, until 800 °C on SiC-DC for instance [4–5, 10–12]. In the present work, this has not been observed because of the substrate chemical composition and microstructure predominant impact. The highest SSA (Table 5) are indeed obtained with oxygen rich fibers (Table 1), etched at lower temperatures (Table 2).

Fiber	SSA ($m^2\ g^{-1}$)	Vol µp ($cm^3\ g^{-1}$)	µp size (Å)	Vol meso ($cm^3\ g^{-1}$)	$V_{p,0.99}$ ($cm^3\ g^{-1}$)	C parameter a.u.
NL101-DC	1710	0.77	8.3	0.056	0.97	420
NL207-DC	1670	0.75	8.2	0.025	0.89	600
Grade-S-DC	860	0.37	6.4	0.011	0.43	5000
Lox-M-DC	1240	0.55	8.2	0.021	0.68	500
ZMI-DC	1500	0.67	8.1	0.020	0.77	480
ZM-DC	1490	0.67	7.6	0.007	0.70	970
AM-DC	1690	0.76	8.3	0.033	0.87	430
Hi-Ni-DC	1180	0.48	6.1	0.001	0.49	3700
ZE-DC	1400	0.60	6.6	0.001	0.62	3400
Hi-Ni-S-DC	1500	0.62	6.1	0.033	0.66	14500
SA3-DC	1320	0.52	6.0	0.049	0.57	6600

Table 5: Data extracted from N_2 physisorption isotherms at 77 K using BET equation, H-K and BJH (from adsorption branch of isotherm) methods, on SiC-based fibers derived carbon.

BET equation [42] can be used to ascertain the degree of interaction between N_2 molecules and sample (adsorbent/adsorbable) via the C parameter [45]. This value is related to the energy of adsorption of the first monolayer: higher C is, more energetically carbon sites are [52, 61]. These values are found to extend from 420 to 14500 (Table 5). CDC obtained by chlorine etching of first-generation fibers show a C parameter ranging from 420 to 970. With a second-generation substrate, this value lies about 3500, whereas highest values are

calculated with third-generation derived carbon. This parameter hence falls when the oxygen content increases. Such phenomenon may infer from energetically carbon sites depletion, caused by partial CDC oxidation by *in-situ* oxygen. The Grade-S-DC does not follow this trend with a C parameter intermediate between second and third generation fiber-derived carbons, showing the singularity of this microporous carbon compared to others.

The narrowest micropores measurable with nitrogen are about 4.5 Å width [44]. For pore width below 7 Å (named ultramicropores), the adsorption is limited to a single step pore filling by a molecular volume of adsorbable (for $P/P_0 \leq 10^{-6}$). However, for larger partial pressure, cooperative and multistep molecular filling of adsorbable volume occurs (for $10^{-6} < P/P_0 \leq 10^{-1}$) in supermicropores. Their respective volumes are revealed by alpha-s method [46–49]. Second and third generation fibers (Hi-Ni, ZE, Hi-Ni-S and SA3) derived carbons exhibit a larger ultramicropores effective volume fraction than supermicropores. Such distinction in micropore sizes is not evidenced on first-generation SiCO fibers derived.

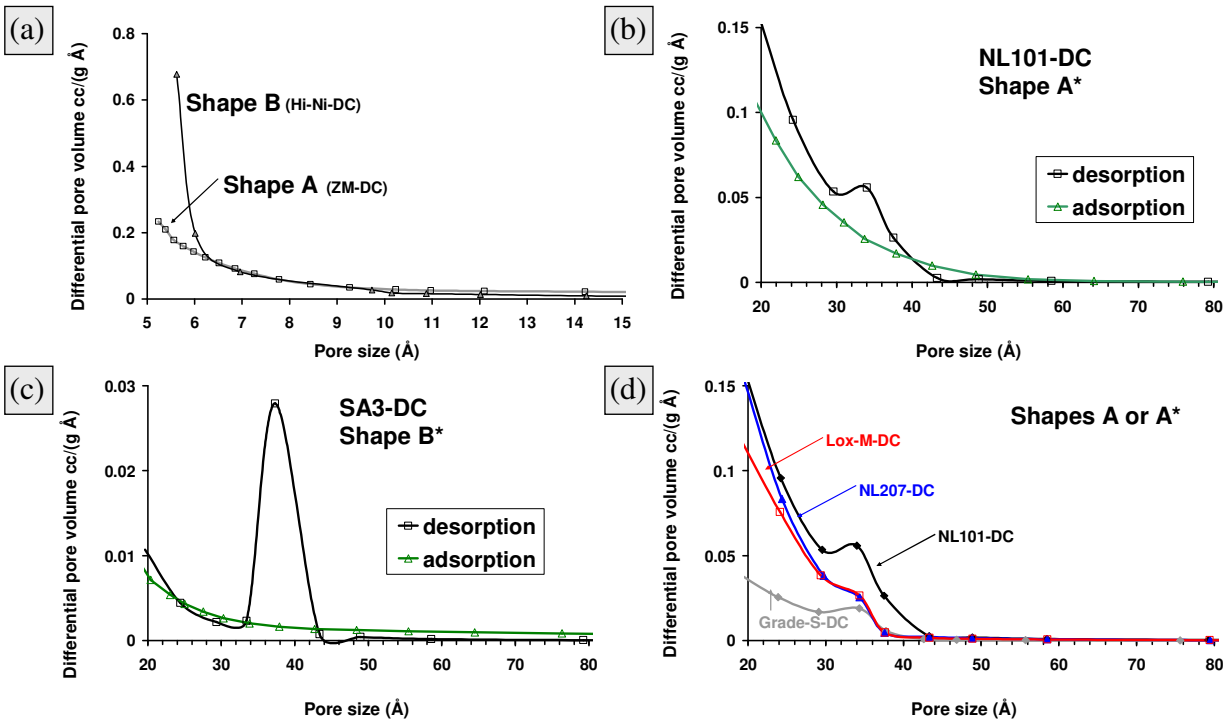

Fig. 3: Pore size distribution of carbon derived from silicon carbide fiber calculated from nitrogen physisorption experiments: (a) micro-PSD using H-K approach with slit pores geometry (b-c), comparison of meso-PSD calculated from adsorption (Δ) and desorption (□) branches of isotherm using BJH method and (e) meso-PSD (calculated from desorption branch of isotherm) of different first-generation fibers.

Shape B* might be ascribed to internal porosity existing in as received fibers and formed during the sintering treatment at high temperature. Adsorption and desorption derived PSD show a progressive decrease from 20 Å (almost micropores) to 30 Å (Figs. 3.c). Even if the PSD derived from adsorption branch is questionable because not in thermodynamic equilibrium and that BJH method is not adapted for pores smaller than 40 Å, this similarity indicates no pore blocking effect drives the desorption of these small mesopores. However, desorption-derived PSD shows a shoulder of artificial pores around 37 Å diameters. This peak is attributed to cavitation phenomenon: the capillary condensate of all coarser pores suddenly and spontaneously evaporates at a given pressure, not dictated by neck size, rather the adsorbate or temperature [62–63]. Therefore, peak at 37 Å observed on shape B* desorption-derived PSD does not correspond to a given size, rather larger mesopores extending to 80 Å or above. The mesoporous volume given in table 5 (accounting for pores larger than 40 Å) is derived from adsorption branch, despite not in thermodynamic equilibrium, for that reason: pore volume ascertained from desorption branch is underestimated. It is generally admitted that BJH method can underestimate the pore size by up to 20-30% for mesorpores smaller than 100 Å [44, 51].

Shape A* shows, like shape B*, a progressive decrease of differential pore volume for smallest mesopores (between 20 and 30 Å) found on adsorption and desorption-derived PSD. A shoulder about 34 Å is observed on PSD calculated from desorption branch. This shoulder is observed on NL101-DC (Fig. 3.b), but also on NL207-DC, Grade-S-DC and Lox-M-DC (Fig. 3.d), even if less obvious on shape A isotherms (Fig. 2.a). The 34 Å mesopores size is not observed on zirconium and aluminum doped fibers (ZMI-DC, ZM-DC and AM-DC) despite similar oxygen content. This peak is, again, purely artificial [62–63] and should not be interpreted as actual mesopore family. Indeed, it results from cavitation effect, independent to neck size, and corresponds to simultaneous evaporation of all larger mesopores capillary condensate [44].

C. Vakifahmetoglu et al. observed micro-mesoporous carbon formed by SiCO chlorination and attributed mesoporosity to domain sizes where silicon has a mixed carbon-oxygen environment [22]. Another origin for these mesopores would be an *in-situ* oxidation of carbon walls separating pores (Equations. 2 and 3), resulting in their fusion. This controlled oxidation can explain the absence of ultramicroporisty on first-generation derived carbon, transformed in supermicropores (between 0.7 and 2 nm pore width) or mesopores (> 2 nm). This

hypothesis meets the following observation: micropore size increases with oxygen content (Tables 1 and 5). These two parameters are otherwise correlated by a logarithmic law (Fig. 4). Indeed, low oxygen content fibers (second and third-generation) show 6-7 Å micropore median width range, whereas first-generation SiCO show it above 7.5 Å. Grade-S-DC does not follow the same tendency.

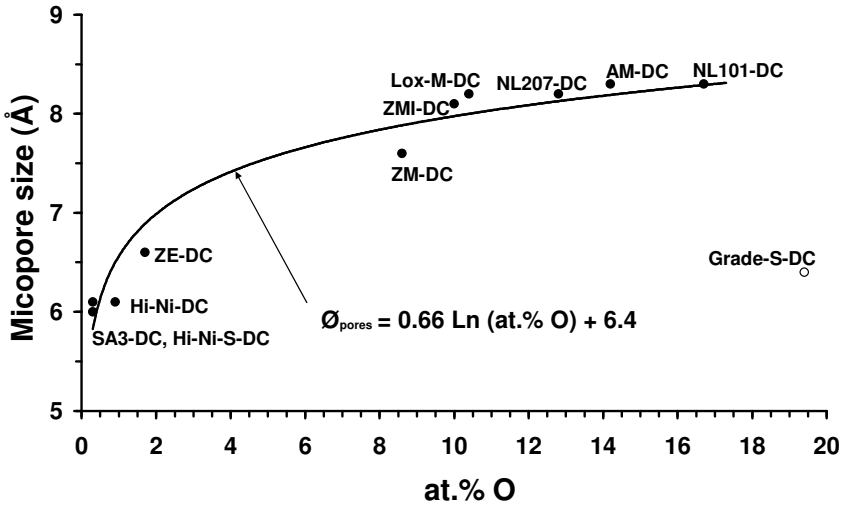

Fig. 4: Relationship between the oxygen content of the as-received SiC fibers and the median micropore size (H-K method) once fully transformed in CDC by chlorination treatment.

The particular case of Grade-S-DC shall now be discussed. This CDC shows an original behavior compared to others. Indeed, despite an oxygen content above the NL101 (Table 1), its equivalent SSA, total pore volume, microporous effective volume and median micropore width are low and its C parameter high. No relevant volume of ultramicroporosity could be highlighted by alphas-s method that could have explained the C value. This fiber derived carbon displays, by far, the highest reactivity among the considered samples for this work [31]. A hypothesis infers from the low transformation temperatures (550 °-575 °C Table 2) used for its transformation: as mentioned, chlorine is thermally desorbed from micropores above 600 °C and ambient pressure, even during the chlorination treatment. Grade-S fiber is the only sample transformed below this temperature threshold. Therefore, chlorine is likely to be partly trapped in CDC while forming, and would avoid, in some way, amorphous carbon organization or rearrangement. This may explain the high C value calculated. During the desorption post treatment, all chlorine species are extracted which could lead to a micro or mesoporosity collapsing, explaining the low effective microporous volume measured (Fig. 4).

3.4 SiC-fiber-DC oxidation kinetics

The oxidation behavior of CDC has been investigated by thermogravimetric analysis (TGA) under pure and dry oxygen. In figure 5, records show the mass loss as a function of temperature for seven (7) fibers derived carbon belonging to all generations. CDC burn-off is observed since 400 °C [12] or even below [29]. Grade-S-DC is clearly the most sensitive to oxidation, behavior consistent with its low synthesis temperature [12] and, as mentioned before, its presumed structural instability. As far as other samples are concerned, results are in accordance with pore structure: the larger the pore size, the higher the accessibility of oxygen is, and thus the faster the burn-off proceeds. Indeed, Hi-Ni-DC (shape B isotherm with narrow PSD) shows the lowest oxidation kinetics whereas SA3-DC and Hi-Ni-S-DC (shape B* isotherm micro-mesoporosity) display a sharp mass loss from 500 °C. CDC with a broad micropore size distribution (shapes A and A*) are intermediate. The effect of heteroelements on oxidation sensitivity could be pointed out but questioned by the different temperatures used for etching treatment. Therefore, the oxidation sensitivity of CDC obtained with different SiC fibers precursors correlates with the porosity structure, mainly the PSD, characterized by N_2 physisorption experiments.

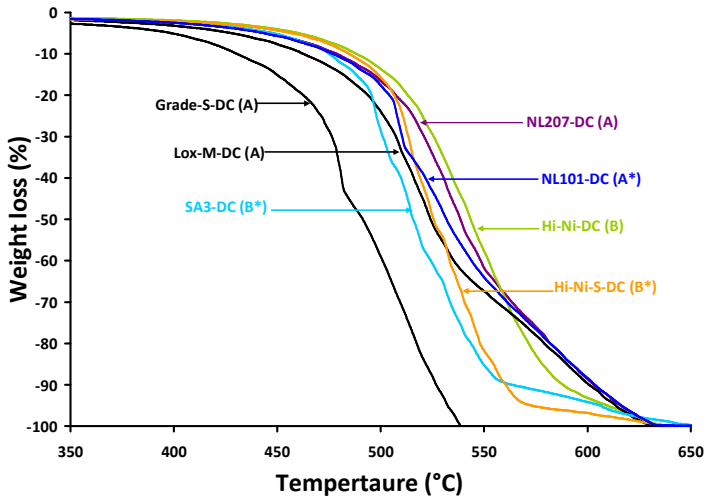

Fig. 5: TGA burn-off curves of silicon carbide based fiber derived carbon, obtained under pure and dry oxygen with a 5 °C min^{-1} heating ramp.

The apparent activation energy of CDC oxidation is calculated from the Arrhenius equation (Equation 9) with k the kinetic constant (s^{-1}), ascertained with the first derivation of the curves in 300 °–500 °C temperature range (Fig. 5). Apparent activation energies are summarized in

table 6 for all studied SiC-fiber-derived carbons. Small differences in reactivity are highlighted between samples. CDC with broadly distributed micropore size (shape A or A* isotherms) show activation energies in the 95−100 kJ mol^{-1} range, excepting when derived from zirconium-doped fibers (no mesoporosity detected on desorption-derived meso-PSD). Carbon derived from second or third-generation fibers show higher activation energies, even when mesoporosity is detected, which is consistent with the free carbon network organization (high temperature pyrolysis process) and, in less extend, with the chlorination temperature. A. Delcamp et al. give apparent activation energy of 120 kJ mol^{-1} for ZMI-DC [17, 29] in accordance with the present work but lower than the ones reported for activated carbon oxidation, more likely about 150−180 kJ mol^{-1} [64]. This parameter seems more likely governed by the fiber synthesis route rather than the PSD.

Shape	Sample	Ea (kJ mol^{-1})	k_0 (s^{-1})
A*	NL101-DC	100	240
A	NL207-DC	100	220
A	Grade-S-DC	98	16
A	Lox-M-DC	96	210
A	ZMI-DC	110	660
A	ZM-DC	160	5.2×10^6
A	AM-DC	100	420
B	Hi-Ni-DC	120	4300
B	ZE-DC	150	2.6×10^5
B*	Hi-Ni-S-DC	180	6.5×10^7
B*	SA3-DC	140	6.0×10^5

Table 6: Data extracted from burn-off TGA experiments under pure dry oxygen on SiC-fiber-derived-carbon.

3.5 SiC-fiber-DC mechanical properties

Mechanical properties of CDC were measured by tensile testing 20 fully transformed SiC monofilaments of each type, extracted from tows chlorinated in the same conditions: 850 °C for 120 min. The CDC displays a brittle behavior (Fig. 6), with average elastic moduli between 7 GPa and 19 GPa and elongation between 0.9% and 4% (Table 7). This former property is larger than the 5 GPa elastic modulus reported and extracted from nano-indentation experiments on β-SiC whiskers derived carbon [16]. The tensile strength is found to drastically drop compared to the as-received fibers. None of these properties seem to be correlated with the porosity structure (Table 5), the initial microstructure or oxygen content (Table 1). Therefore, the differences between CDC mechanical properties found a different origin.

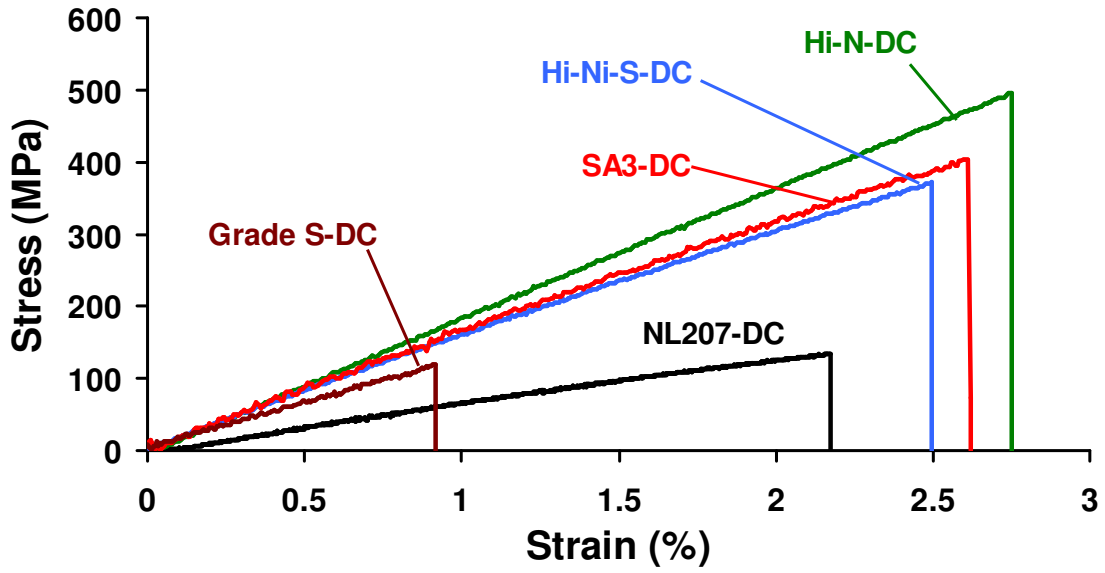

Fig. 6: Tensile strain-stress curves of different SiC-based monofilaments, fully transformed in CDC by chlorination treatment at 850 °C for 120 min.

Samples	Experimental properties ± std. dev.			Calculated
	Tensile strength (MPa)	Elongation (%)	Young modulus (GPa)	E (mixture rule) (GPa)
NL101-DC	168 ± 45	1.5 ± 0.8	11 ± 2.3	13.6
NL207-DC	130 ± 50	2.1 ± 0.8	7.0 ± 2	12.7
Grade-S-DC	130 ± 45	0.9 ± 0.3	14 ± 2.9	16.1
Lox-M-DC	310 ± 75	2.1 ± 0.8	13 ± 1.0	16.3
ZMI-DC	330 ± 45	2.8 ± 0.4	12 ± 1.5	16.7
ZM-DC	480 ± 130	3.0 ± 0.7	16 ± 2.2	17.5
AM-DC	240 ± 60	2.1 ± 0.9	11 ± 1.5	16.8
Hi-Ni-DC	510 ± 75	2.8 ± 0.4	19 ± 1.5	14.0
ZE-DC	670 ± 150	4.0 ± 0.8	16 ± 1.9	17.7
Hi-Ni-S-DC	370 ± 75	2.5 ± 0.6	16 ± 2.0	8.5
SA3-DC	420 ± 140	2.4 ± 0.9	16 ± 2.6	8.5

Table 7: Mechanical properties of carbon-derived from SiC fibers measured by tensile tests.

The CDC tensile strength seems however correlated to the electrical conductivity of as-received fibers (Fig. 7). Hi-Ni-S-DC is found to slightly differ from this behavior. As mentioned before, electrical conductivity characterizes the percolation state of the BSU. This correlation means the tensile strength of CDC reflects the continuity of former carbon free network, as it is the only phase remaining intact after the chlorination treatment [13]. This

observation raises an original method to analyze and quantify the percolation of carbon free phase in SiC fibers.

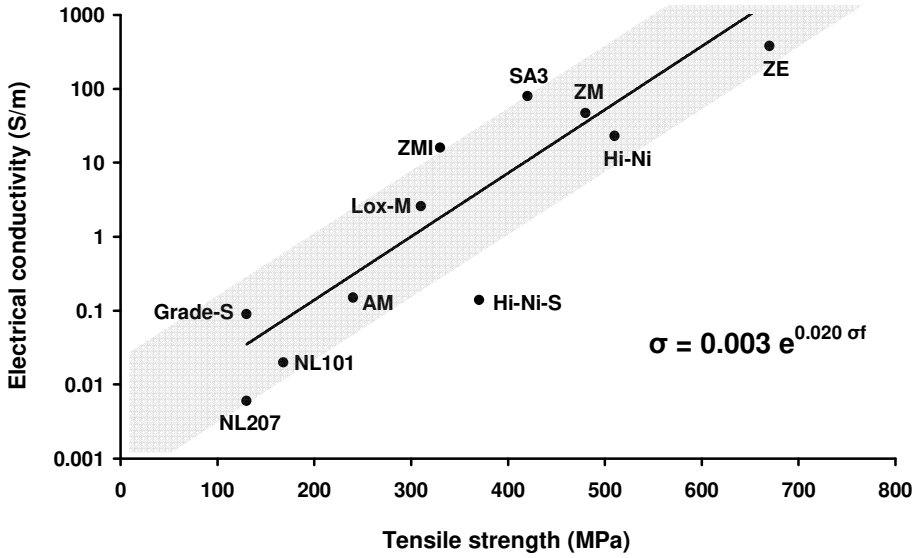

Fig. 7: Relationship between the electrical conductivity (σ) of as-received SiC-fibers and the tensile strength (σ_f) of corresponding CDC after 120 min chlorination at 850 °C.

CDC Young modulus is likely to follow the mixture rule. As an assumption, Young moduli of carbon free network, amorphous carbon-derived from SiC and from SiCO, are respectively considered to be 28 GPa, 5 GPa [16] and negligible (E_{SiCO} = 0 GPa). Considering the volume proportions given in table 1, third-generation fibers (Hi-Ni-S-DC and SA3-DC), and in a lower extend the Hi-Ni-DC, show a lower calculated modulus (Table 7). This observation is consistent with as-received fibers results presented in table 3 and attributed to the underestimation of the C_{free} modulus after higher temperature pyrolysis. The Young modulus extracted from tensile tests on all other fibers derived carbons, is close but lower than the ones calculated by the mixture rule (Table 7). An overestimation of the C_{free} modulus could here be pointed out.

Therefore, mechanical properties of CDC can be used to estimate the free carbon amount using the mixture rule, as well as its percolation, linked to the electrical conductivity of former SiC-based fibers. Hence, tensile test of SiC-fibers-DC could be simplified to the characterization of the carbon free network, embedded into amorphous carbon with poor mechanical properties. The similarity with composite materials, here carbide or oxycarbide-derived carbon reinforced with sp2 carbon network, can thus be proposed. It is worth noting

the considered modulus and the volume fraction in the mixture rule are indirectly assessed and do not account for the synthesis temperature. This calculation can therefore be misleading, whereas the electrical conductivity is a direct measurement. Such result could be used to target some mechanical properties of CDC for the desired application. The carbon free amount can for example be adjusted in SiCO glasses by process settings [13].

4. Conclusion

A large number of silicon carbide fibers, covering a wide range of chemical compositions and microstructures, were fully converted into porous carbon by selective etching of silicon atoms with chlorine in the temperature range 550 °-850 °C. These materials were mostly microporous with high equivalent specific surface area (> 1000 m^2 g^{-1}). Carbon derived from third-generation fibers highlighted some mesoporosity, likely formed during fibers sintering process. The pore size was found to be correlated to the oxygen content of as-received fibers: second and third generation fibers gave carbon revealing ultramicroporosity (width < 7 Å) whereas carbon derived from first-generation fibers showed pore enlargement, up to mesopores. This was attributed to nano-domains of mixed silicon environment or to the *in-situ* oxidation of carbon walls, decreasing in the mean while the C parameter. The PSD difference (mesoporosity detection) between titanium or aluminum and zirconium doped fibers-CD did not found clear explanation and would need further dedicated investigations. Grade-S-DC did not follow the trend with limited mesoporosity, low SSA and high value of C, despite its former high oxygen content. This could be ascribed to its high chemical reactivity and associated low transformation temperature, limiting chlorine desorption during the treatment and, presumably, preventing carbon organization.

The oxidation of CDC was observed since 400 °C but all samples did not follow the same kinetic; behavior correlated with the accessibility of oxygen to the carbon and thus to the PSD. The oxidation apparent activation energy was found to range from 95 to 180 kJ mol^{-1}. This property could be linked to free carbon BSU organization in as-received fibers and thus their manufacturing process.

Mechanical properties of CDC were tuned by free carbon excess in the former materials: the tensile strength was linked to its percolation state whereas the Young modulus was attributed to its amount and organization. This former statement was deduced from the relationship existing between electrical conductivity and tensile strength of respectively as-received and transformed fibers. The later statement, concerning the relationship between carbon free amount and CDC elastic modulus, resulted from the relevancy of the mixture rule considering

a 28 GPa modulus for carbon free, 5 GPa for SiC-DC and neglecting the SiCO-DC one. These materials can be associated to amorphous carbon matrix composites reinforced by aromatic carbon.

As known, CDC are unique materials offering the possibility to fine tune the pore size distribution, from micro to mesopores, by proper substrate selection or treatment condition adjustment. The oxidation sensitivity of such materials makes them inappropriate for application in oxidizing environment at temperatures exceeding 400 °C, even 300 °C for long duration. Their shape memory, offered by small diameter fibers, and their mechanical properties however did not retained attention of previous studies. The latter can be adjusted using a sub-network of etching-inert materials (for instance, carbon, silica, alumina can be selected against chlorine) embedded in the carbide matrix. This opens a new investigation field for CDC future development in mechanically stressed applications.

Acknowledgment

The authors acknowledge R. Denoyel for editorial advices and the financial support of the Snecma Propulsion Solide (now Safran Ceramics) for this work.

Data availability

The raw/processed data required to reproduce these findings cannot be shared at this time due to technical or time limitations.

References

[1] Yushin G, Nikitin A, Gogotsi Y. Carbide-derived carbon. In: Gogotsi Y, editor. Nanomaterials Handbook. CRC Taylor&Francis. 2006; 239–82.
doi: 10.1002/anie.200685445

[2] Lee A, Zhu R, McNallan MJ. Kinetics of conversion of silicon carbide to carbide derived carbon. J Phys Cond Matter 2006; 18:1763–70.
doi: 10.1088/0953-8984/18/32/S07

[3] Gogotsi Y, Jeon ID, McNallan MJ. Carbon coating s on silicon carbide by reaction with chlorine-containing gases. J Mater Chem 1997; 7(9):1841–48.
doi: 10.1039/A701126A

[4] Ishikawa S, Saito T, Kuwahara K. Carbon Materials with Nano-sized Pores Derived from Carbides. SEI Tech Review 2016:152–7.

[5] Gogotsi Y, Dash RK, Yushin G, Yildirim T, Laudisio G, Fischer JE. Tailoring of nanoscale porosity in carbide-derived carbons for hydrogen storage. J Am Ceram Soc 2005; 127(46):16006–7.
doi: 10.1021/ja0550529

[6] Dash RK, Yushin G, Gogotsi Y. Synthesis, structure and porosity analysis of microporous and mesoporous carbon derived from zirconium carbide. Microp Mesop Mater 2006; 86:50–7.
doi: 10.1016/j.micromeso.2005.05.047

[7] Dimovski D, Nikitin A, Ye H, Gogotsi Y. Synthesis of graphite by chlorination of iron carbide at moderate temperatures. J Mater Chem 2004; 14:238–43.
doi: 10.1039/b311938f

[8] Kukushkina YA, Sokolov VV, Tomkovich MV. Nanoporous carbon prepared by thermochemical treatment of carbide with chlorine. Russ J Appl Chem 2014; 87(10):1517–23.
doi: 10.1134/S107042721410019X

[9] Urbonaite S, Juarez-Galan JM, Leis J, Rodriguez-Reinoso F, Svensson G. Porosity development along the synthesis of carbons from metal carbides. Microp Mesop Mater 2008; 113:14–21.
doi: 10.1016/j.micromeso.2007.10.046

[10] Gogotsi Y, Nikitin A, Ye H, Zhou W, Fisher JE, Yi B, et al. Nanoporous carbide-derived carbon with tunable pore size. Nature Materials 2003; 2:591–594.
doi: 10.1038/nmat957

[11] Chmiola J, Yushin G, Gogotsi Y, Portet C, Simon P, Taberna PL. Anomalous increase in carbon capacitance at pore sizes less than 1 nanometer. Science 2006; 313:1760–3.
doi: 10.1126/science.1132195

[12] Kormann M, Gehard H, Popovska N. Comparative study of carbide-derived carbons obtained from biomorphic TiC and SiC structures. Carbon 2009; 47(1):242–50.
doi: 10.1016/j.carbon.2008.10.002

[13] Yeon SH, Eddington P, Gogotsi Y, Fischer JE, Vakifahmetoglu C, Colombo P. Carbide-derived-carbons with hierarchical porosity from a preceramic polymer. Carbon 2010; 48(1):201–10.
doi: 10.1016/j.carbon.2009.09.004

[14] Popovska N, Kormann M. Processing of porous carbon with tunable pore structure by the carbide-derived carbon method. JOM 2010; 62-6:44–49.
doi: 10.1007/s11837-010-0086-7

[15] Duan L, Ma Q, Chen Z. Etching process of silicon carbide from polysiloxane by chlorine. Corr Sci 2014; 87:127–133.
doi: 10.1016/j.corsci.2014.06.014

[16] Chen L, Behlau G, Gogotsi Y, McNallan MJ. Carbide derived carbon (CDC) coatings for Tyranno ZMI SiC fibers. Ceram Eng Sci Proc 2003; 24:57–62.
doi: 10.1002/9780470294802.ch8

[17] Delcamp A, Maille L, Rufino B, Mazerat S, Pailler R, Guette A, et al. In-situ processing of carbon coating on the surface of SiC-based fibers. Surf Coat Tech 2010; 205(3):703–9. doi: 10.1016/j.surfcoat.2010.07.060

[18] Brisebourg M, Mazerat S, Puyoo G, Plaisantin H, Dibandjo P, Soraru GD, et al. Si-C-O fibres in gas reactive atmospheres. Adv Sci Tech 2010; 71:86–91. doi: 10.4028/www.scientific.net/AST.71.86

[19] Rufino B, Mazerat S, Couvrat M, Lorette C, Maskrot H, Pailler R. The effect of particle size on the formation and structure of carbide-derived carbon on β-SiC nanoparticles by reaction with chlorine. Carbon 2011; 49(9):3073–83. doi: 10.1016/j.carbon.2011.03.029

[20] Cambaz ZG, Yushin GN, Gogotsi Y. Formation of carbide-derived carbon on β-silicon carbide wiskers. J Am Ceram Soc 2006; 89(2):509–14. doi: 10.1111/j.1551-2916.2005.00780.x

[21] Batisse N, Guerin K, Dubois M, Hamwi A. The synthesis of microporous carbon by the fluorination of titanium carbide. Carbon 2011; 49(9):2998–3009. doi: 10.1016/j.carbon.2011.03.018

[22] Vakifahmetoglu C, Presser V, Yeon SH, Colombo P, Gogotsi Y. Enhanced hydrogen and methane gas storage of silicon oxycarbide derived carbon. Microp Mesop Mater 2011; 144:105–112. doi: 10.1016/j.micromeso.2011.03.042

[23] Osswald S, Portet C, Gogotsi Y, Laudisio G, Singer JP, Fischer JE, et al. Porosity control in nanoporous carbide-derived carbon by oxidation in air and carbon dioxide. J Solid State Chem 2009; 182:1733–41. doi: 10.1016/j.jssc.2009.04.017

[24] Kormann M, Popovska N. Processing of carbide-derived carbons with enhanced porosity by activation with carbon dioxide. Microp Mesop Mater 2010; 130:167–73.

doi: 10.1016/j.micromeso.2009.10.028

[25] Schmirler M, Glenk F, Etzold BJM. In-situ thermal activation of carbide-derived carbon. Carbon 2011; 49(11):3679–86.
doi: 10.1016/j.carbon.2011.05.003

[26] Portet C, Lillo-Rodenas MA, Linares-Solano A, Gogotsi Y. Capacitance of KOH activated carbide-derived carbons. Phys Chem Chem Phys 2009; 11:4943–5.
doi: 10.1039/B816514A

[27] Welz S, McNallan MJ, Gogotsi Y. Carbon structures in silicon carbide derived carbon. J Mater Proc Tech 2006; 179:11–12.
doi: 10.1016/j.jmatprotec.2006.03.103

[28] Gogotsi Y, Welz S, Daghfal J, McNallan MJ, Jeon ID, Nickel KG. Formation of carbon coating on SiC fibers by selective etching in halogens and supercritical water. Ceram Eng Sci Proc 1998; 19(3)87–94.
doi: 10.1002/9780470294482.ch10

[29] Delcamp A. Protection de fibres base SiC pour composites à matrice céramique. University of Bordeaux France, PhD thesis, 2008.

[30] Mazerat S. Fibre de renfort pour composites SiC/SiC : amélioration et corrélation de la durée de vie sous air à T<900°C avec la réactivité chimique. University of Bordeaux France, PhD thesis, 2012.

[31] Mazerat S, Puyoo G, Chollon G, Teyssandier F, Pailler R, Loison S, et al. Composition and reactivity of various silicon carbide fibers. HTCMC8 Ceram Trans 2014; 248:113–123.
doi: 10.1002/9781118932995.ch13

[32] Presser V, Heon M, Gogotsi Y. Carbide-Derived Carbons – From Porous Networks to Nanotubes and Graphene. Adv Funct Mater 2016; 21(5):810–33.
doi: 10.1002/adfm.201002094.

[33] Ersoy D, McNallan MJ, Gogotsi Y, Erdemir A. Tribological properties of carbon coatings produced by high temperature chlorination of silicon carbide. STLE Tribol Trans 2000; 43:809–15.
doi: 10.1080/10402000008982412

[34] Chun YS, Lim DS. Carbide derived carbon: from growth to tribological application. J Ceram Soc Jap 2014; 122(8):577–85.
doi: 10.2109/jcersj2.122.577

[35] McNallan MJ, Ersoy DA, Zhu R, Lee A, White C, Welz C, et al. Nano-Structured Carbide Derived Carbon (CDC) Films and their Tribology. Tsinghua Sci Technol 2005; 10:699–703.
doi: 10.1016/S1007-0214(05)70138-3

[36] Chen X, Cantrell DR, Kohlhaas K, Stankovich S, Ibers JA, Jaroniec M, et al. Carbide-Derived Nanoporous Carbon and Novel Core-Shell Nanowires. Chem Mater 2006; 18:753–8.
doi: 10.1021/cm051991o

[37] Laffon C, Flank AM, Lagarde P, Laridjani M, Hagege R, Orly P, et al. Study of Nicalon-based ceramic fibres and powders by EXAFS spectrometry, X-ray diffractometry and some additional methods. J Mater Sci 1989; 24:1503–12.
doi: 10.1007/BF02397093

[38] Flores O, Bordia RK, Nestler D, Krenkel W, Motz G. Ceramic Fibers Based on SiC and SiCN Systems: Current Research, Development, and Commercial Status. Adv Eng Mater 2014;16(6):621–36.
doi: 10.1002/adem.201400069

[39] Teyssandier F, Puyoo G, Mazerat S, Chollon G, Pailler R, Babonneau F. Contribution to the understanding of the microstructure of first generation Si–C–O fibers. Ceram Eng Sci Proc 2013; 33(8):1–10.
doi: 10.1002/9781118217528.ch1

[40] Ersoy DA, McNallan MJ, Gogotsi Y. Carbon coatings produced by high temperature chlorination of silicon carbide ceramics. Mater Res Innovat 2001; 5(2):55–62.
doi: 10.1007/s100190100136

[41] Chollon G, Pailler R, Canet R, Delhaes P. Correlation between microstructure and electrical properties of SiC-based fibres derived from organosilicon precursors. J Eur Ceram Soc 1998; 18:725–33.
doi: 10.1016/S0955-2219(97)00177-5

[42] Brunauer S, Emmett PH, Teller E. Adsorption of gases in multimolecular layers. J Am Chem Soc 1938; 60:309–19.
doi: 10.1021/ja01269a023

[43] Horvath G, Kawazoe K. Method for the calculation of effective pore size distribution in molecular sieve carbon. J Chem Eng Japan 1983; 16(6):470–75.
doi: 10.1252/jcej.16.470

[44] Thommes M. Physical Adsorption Characterization of Nanoporous Materials. Chem Ing Tech 2010; 82(7):1059–73.
doi: 10.1002/cite.201000064

[45] Sing KSW, Everett DH, Haul RAW, Moscou L, Pierotti RA, Rouquerol J, et al. Reporting physisorption data for gas/solid systems. Pure App Chem 1985; 57(4):603–619.
doi: 10.1351/pac198254112201

[46] Sing KSW. Empirical method for analysis of adsorption isotherms. Chem Ind 1968; 44:1520–1.

[47] Sing KSW. Surface Area Determination. Everett, D.H., Ottewill, R.H., Eds, Butterworths, London, 1970; 15.

[48] Sing KSW. The use of physisorption for the characterization of microporous carbons. Carbon 1989; 27(1):5–11.
doi: 10.1016/0008-6223(89)90151-6

[49] Sing KSW. The use of gas adsorption for the characterization of porous solids. Colloids Surf 1989; 38(1):113–24.
doi: 10.1016/0166-6622(89)80148-9

[50] Silvestre-Albero A, Silvestre-Albero J., Martınez-Escandell M., Futamura R., Itoh T., Kaneko K., et al. Non-porous reference carbon for N2 (77.4 K) and Ar (87.3 K) adsorption. Carbon 2014;6:699–794
doi: 10.1016/j.carbon.2013.09.068

[51] Barrett EP, Joyner LG, Halenda PP. The determination of pore volume and area distributions in porous substances. I. Computations from nitrogen isotherms. J Am Chem Soc 1951; 73:373–80.
doi: 10.1021/ja01145a126

[52] Thommes M, Kaneko K, Neimark AV, Olivier JP, Reinoso FR, Rouquerol J, et al. Physisorption of gases, with special reference to the evaluation of surface area and pore size distribution (IUPAC Technical Report). Pure App Chem 2015; 87(9-10).
doi: 10.1515/pac-2014-1117

[53] Mazerat S, Delcamp A, Pailler R, Lamon J, Plaisantin H. Improvement of silicon carbide fibers mechanical properties by Cl_2 etching. J Eur Ceram Soc 2018; 38(16):5301–10.
doi: 10.1016/j.jeurceramsoc.2018.06.026

[54] Lissart N, Lamon J. Statistical analysis of failure of SiC fibres in the presence of bimodal flaw populations. J Mater Sci 1997; 32:6107–17.
doi: /10.1023/A:1018600119250

[55] Li CT, Tietz JV. Improved accuracy of the laser diffraction technique for diameter measurement of small fibres. J Mater Sci 1990; 25(11):4694–8.
doi: 10.1007/BF01129926

[56] Bunsell AR, Piant A. A review of the development of three generations of small diameter silicon carbide fibres. J Mater Sci 2006; 41:823–39.

doi: 10.1007/s10853-006-6566-z

[57] Le Coustumer P, Monthioux M, Oberlin A. Understanding Nicalon Fibre. J Eur Ceram Soc 1993; 11:95–103.
doi: 10.1016/0955-2219(93)90040-X

[58] Dong SM, Chollon G, Labrugere C, Lahaye M, Guette A, Bruneel JL, et al. Characterization of nearly stoichiometric SiC ceramic fibres. J Mater Sci 2001; 36:2371–81.
doi: 10.1023/A:1017988827616

[59] Gogotsi Y. Nanomaterials Handbook, Gogotsi Y, Editor. 2006, CRC Press.

[60] Gregg SJ, Sing KSW. Adsorption, Surface Area and Porosity, Academic Press, London, 1982.
doi: 10.1002/bbpc.19820861019

[61] Sing KSW. The use of nitrogen adsorption for the characterisation of porous materials. Coll Surf A Physicochemical Eng Aspects 2001; 187–188:3–9.
doi: 10.1016/S0927-7757(01)00612-4

[62] Groen JC, Peffer LAA, Pérez-Ramírez J. Pore size determination in modified micro- and mesoporous materials. Pitfalls and limitations in gas adsorption data analysis. Microp Mesop Mater 2003; 60:1–17.
doi: 10.1016/S1387-1811(03)00339-1

[63] Bertier P, Schweinar K, Stanjek H, Ghanizadeh A, Clarkson CR, Busch, A et al. On the use and abuse of N_2 physisorption for the characterization of the pore structure of shales. CMS Workshop Lectures 2016; 21:151–61.
doi: 10.1346/CMS-WLS-21.12

[64] Smith IW. The intrinsic reactivity of carbons to oxygen. Fuel 1978;57:409–14.
doi: 10.1016/0016-2361(78)90055-8